CONDENSED MATTER PHYSICS

Fast equilibration mechanisms in disordered materials mediated by slow liquid dynamics

Zijian Song†, Cristian Rodríguez-Tinoco†‡, Allen Mathew, Simone Napolitano*

The rate at which a nonequilibrium system decreases its free energy is commonly ascribed to molecular relaxation processes, arising from spontaneous rearrangements at the microscopic scale. While equilibration of liquids usually requires density fluctuations at time scales quickly diverging upon cooling, growing experimental evidence indicates the presence of a different, alternative pathway of weaker temperature dependence. Such equilibration processes exhibit a temperature-invariant activation energy, on the order of 100 kJ mol^{-1}. Here, we identify the underlying molecular process responsible for this class of Arrhenius equilibration mechanisms with a slow mode (SAP), universally observed in the liquid dynamics of thin films. The SAP, which we show is intimately connected to high-temperature flow, can efficiently drive melts and glasses toward more stable, less energetic states. Our results show that measurements of liquid dynamics can be used to predict the equilibration rate in the glassy state.

INTRODUCTION

The properties of a collection of objects at thermodynamic equilibrium do not change with time. Experience tells us that such observation is, however, rarely encountered in nature. The transformation of buds into flowers and then fruits, the rearrangements of plates on the surface of planets, and even the whole human body over its lifetime are just a few, among the many, examples of systems far from thermodynamic equilibrium.

At the molecular level, equilibration kinetics—the time evolution of a system's properties toward a less energetic state—are intimately coupled to molecular motion. In line with the Onsager's regression hypothesis (*1*), the macroscopic relaxation of a nonequilibrium system (dissipation) obeys the same laws of molecular dynamics in equilibrium conditions (spontaneous microscopic fluctuations). Under such framework, albeit often separated by several orders of magnitude, the rates of macroscopic [equilibration kinetics (t_{eq}^{-1})] and microscopic [molecular motion (t_{mol}^{-1})] processes are strongly correlated and share the same activation energy (=$R\partial lnt/\partial T^{-1}$, where R is the gas constant), that is, $t_{eq}/t_{mol} = c$, where c is a temperature-independent constant (*2*, *3*). On the basis of the latter relation, controlling the equilibration rate—either toward a global or a local minimum in free energy—requires identifying the molecular mechanism that is coupled to the macroscopic equilibration and its efficiency, c.

Equilibration of polymer melts, and, in general, of supercooled liquids, typically follows the structural (segmental, α-) relaxation. This molecular process exhibits a super-Arrhenius temperature dependence (*4*) expressed by an activation energy which increases upon cooling. Examples of this type of equilibration kinetics are the formation of crystals (*5*), the relaxation of nonequilibrium conformations in polymer melts [reptation (*6*) and Fischer modes (*7*)], and, in nanoconfined systems, the recovery of bulk behavior mediated by interfacial layers (*2*, *8*). The physics of such processes is described by density fluctuations occurring within molecular clusters growing upon cooling (*9*, *10*).

Although the super-Arrhenius mechanism is a universal signature linking the equilibrium and the nonequilibrium liquid state, current equilibration frameworks—based on the segmental relaxation only—cannot explain how materials can also fast-equilibrate (days and weeks) when held below the glass transition temperature (*11*–*14*), T_g, a regime where the conventional structural pathway would require geological times. In this regard, an increasing number of experimental observations hint at the presence of a different equilibration pathway, active from well above to well below T_g, with a temperature-invariant activation energy, $E_A \approx 100$ kJ mol^{-1}.

The presence of these anomalous Arrhenius equilibration mechanisms in the liquid state was, for example, reported by probing the crystal growth rate of small molecules (*15*, *16*), the rheological behavior of polymer melts in bulk and upon confinement at the nanoscale level (*17*, *18*), and the desorption and the adsorption of macromolecules on solid substrates, both in silico (*19*) and on real surfaces (*20*). Understanding the nature of these unusual equilibration processes has strong implications. In the design of new materials and their fabrication protocols, a better control of properties is achieved by identifying those conditions favoring mechanisms of weaker temperature dependence (*21*). Moreover, as most raw and processed amorphous materials are stored in the glassy state, the shelf time of these systems is affected by potential equilibration through this alternative pathway.

On the basis of Onsager's regression hypothesis, a molecular mechanism whose activation energy matches that of these macroscopically observed Arrhenius equilibration processes should exist. Considering their weak temperature dependence and their relevance below T_g, possible candidates could be the so-called secondary relaxation processes (β-, γ-, ...), characteristic of the glassy state and attributed to localized motion of a small number of atoms. Until now, the search for this elusive molecular process has, however, been unfruitful. No known relaxation process in the glassy state fits the requirements.

Here, we provide direct experimental evidence on the universal occurrence of slow Arrhenius processes (SAPs) in the liquid dynamics.

Laboratory of Polymer and Soft Matter Dynamics, Experimental Soft Matter and Thermal Physics (EST), Université libre de Bruxelles (ULB), Brussels 1050, Belgium.
*Corresponding author. Email: snapolit@ulb.ac.be
†These authors contributed equally to this work.
‡Present address: Departamento de Física, Facultat de Ciències, Universitat Autònoma de Barcelona and Catalan Institute of Nanoscience and Nanotechnology (ICN2), CSIC and BIST, 08193 Barcelona, Spain.

For each system investigated, the molecular (SAP) and the equilibration processes share the same activation energy, which hint at a common molecular origin. We demonstrate that, independently of the chemical nature, measurements of molecular mobility within the liquid predict the equilibration of systems in the glassy state.

RESULTS

Experimental observation of SAPs in the dielectric response of the liquid state

In Fig. 1, we show the three-dimensional (3D) plot of the dielectric loss (ε'' versus log$f$ versus T) of a 76-nm-thin spin-coated film of polycarbonate (PC), together with isothermal spectra at a temperature well above the glass transition of the system. The time scale of molecular motion is straightforwardly determined by the maxima (*22*) of the frequency peaks (f_{max}) through the relation $t_{mol} = (2\pi f_{max})^{-1}$; see Materials and Methods for further information on data analysis. A relaxation map (logt_{mol} versus T^{-1}) with the characteristic time of the two molecular processes is provided in Fig. 2A. The α-relaxation, associated with segmental motion, moves through the whole frequency range within just 30 K; this feature indicates a high value of thermal activation energy (>400 kJ mol^{-1}). A second peak of lower but constant activation energy (≈ 90 kJ mol^{-1}), crossing the α-relaxation at temperatures above T_g (around 0.1 to 100 Hz, corresponding to the 10^{-3} to 1 ms of time window), is visible over a much larger temperature range (>100 K).

Differently from what is observed for secondary processes, the activation energy and the intensity of the slower peak do not seem affected by the proximity to the α-process. Furthermore, in the frequency domain, this peak is sharper (full width at half height ≈ 1.1 decades) than the α-relaxation (≈2.5 decades) and, by far, less broad than secondary relaxations in the glassy state [the β-relaxation of PC (*23*) extends for more than 5 decades and has an activation energy ≈30 kJ mol^{-1}].

Within experimental uncertainties, this SAP can be associated to the spectral response of a molecular mechanism with a single relaxation time, ~$(1 + 2\pi f t_{mol})^{-1}$, corresponding to a simple exponential decay in the time domain, exp($- t/t_{mol})^{\beta_{KWW}}$, with $\beta_{KWW} = 1$. Debye associated such sharp peaks to the dielectric response of a gas of dipole moments, corresponding to an ensemble of noninteracting identical relaxation units (*24*, *25*).

Processes with the same characteristics that we ascribe to the SAP (constant activation energy, $\beta_{KWW} \approx 1$, crossing the α-process above T_g) were observed for all the other investigated polymer systems; see Fig. 2, where we plot the relaxation maps of nine different polymers [see fig. S1 for further examples of isothermal dielectric spectra, fig. S2 (B to I) for the 3D plots of the systems, fig. S3 for a statistical analysis of β_{KWW} of the SAP, and fig. S4 for the relaxation maps of a larger selection of polymers]. For polystyrene (PS), SAPs with the same activation energy that we found in spin-coated thin samples were also observed in the dynamics of bulk melt samples; the results from this work are plotted together with our own results in the figure (see Fig. 2C) (*26*).

By analyzing polymer chains of different molecular weight (from 43 to 6000 kg mol^{-1}) and films of different thickness (h = 7 nm to 100 μm), we verified that this process is also present in bulk melts (h > 200 nm) and that the activation energy and the characteristic molecular time of the SAPs (see figs. S5 and S6) are not affected by either the macromolecular or the sample size. This feature permitted us to discriminate between possible classes of relaxation mechanisms and to discard diffusion-limited processes (*27*), nucleation-driven processes (*28*), and polymer-specific modes (*29*), whose characteristic time would, instead, change with film thickness and molecular weight.

Furthermore, as the position of the SAP peaks is invariant with sample size even in those cases where the α-process shifts upon confinement (see, for example, PC and P4ClS poly(4-chlorostyrene) in Fig. 2), we conclude that the SAPs are related to a genuine molecular mechanism, totally decoupled from that of segmental motion in proximity of the glass transition. On the other hand, we note that the intensity of the SAP process decreases upon confinement (see fig. S7), following the same scaling commonly observed for the

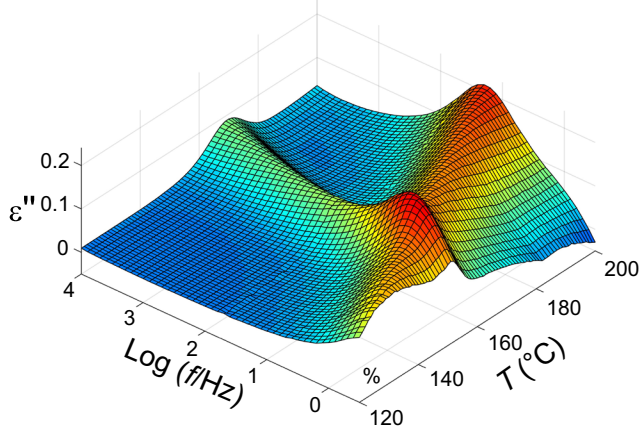

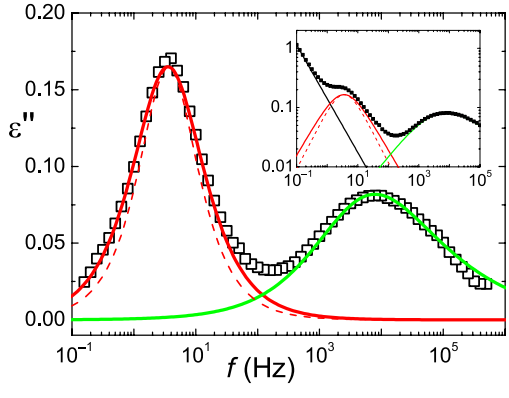

Fig. 1. Experimental signature of slow processes in the liquid state. (**Left**) 3D plot of the dielectric loss (free from conductivity; see below) of a 76-nm film of PC, as a function of temperature and frequency. Relaxation processes appear as peaks shifting toward higher frequency with increasing temperature. Using a model-free approach, the maximum of the relaxation peaks (f_{max}) provides the characteristic time of the molecular process, via the relation $t_{mol} = (2\pi f_{max})^{-1}$. The segmental dynamics (process more parallel to frequency axis) crosses the SAP around 0.1 Hz and 155°C. (**Right**) Isothermal spectrum of the dielectric loss at 169°C; the contribution of conductivity (black line in the inset) was removed for clarity. Two distinct peaks are present, the segmental process (green line) and the SAP (red solid line) at lower frequencies. The latter can be fitted to a symmetric peak, corresponding to a stretching exponent $\beta_{KWW} = 0.9$; a peak with $\beta_{KWW} = 1.0$ (red dashed line) is also plotted for comparison.

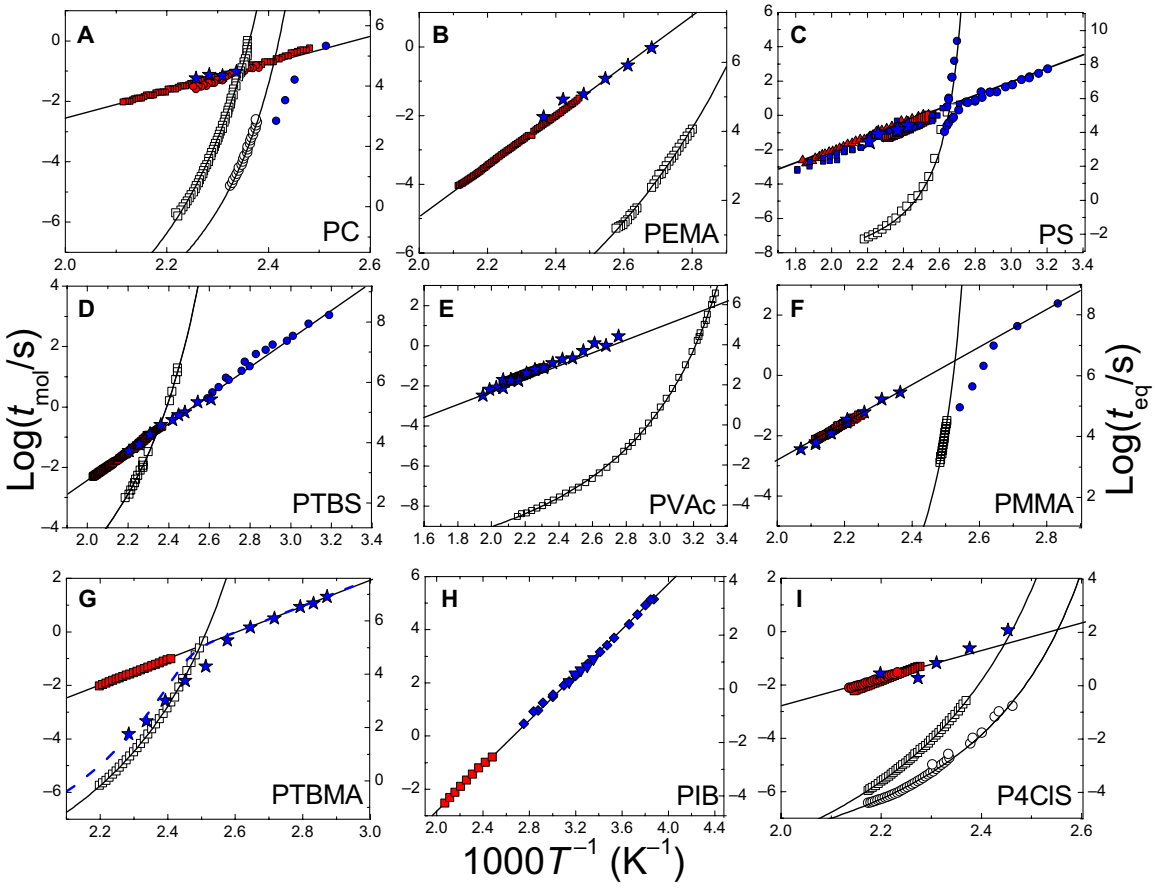

Fig. 2. Relaxation and equilibration maps. (**A** to **I**) To ease visual comparison, we converted equilibration rates into times. For each system, the logarithm of the molecular times (t_{mol}) on the left axes and the logarithm of the equilibration times (t_{eq}) on the right axes are given as a function of the inverse temperature. This representation provides a direct access to the activation energy of the processes (=$R\partial lnt/\partial T^{-1}$, where R is the gas constant). For each polymer, we identify two molecular processes, the segmental relaxation (white symbols) and the SAP (red symbols): Squares were used for bulk samples of >200 nm and circles for thin films (20 nm thin for PC and 7 nm thin for P4ClS); for PS, we also show the time scale of a similar molecular process present in bulk melts (triangles; C) (*26*). Segmental relaxation times of PVAc (polyvinyl acetate) are from (*55*) and of poly(4-tertbutyl styrene) (PTBS) from (*13*). Equilibration data are indicated with blue symbols [stars for adsorption; circles for physical aging of PC (*56*), polystyrene (PS) (*13*, *57*), poly(methyl methacrylate) (PMMA) (*35*), and poly(4-tertbutyl styrene) (PTBS) (*14*); squares for dewetting of PS (*18*); inversed triangles for reentanglement kinetics of polyisobutadiene (PIB) (*30*); and diamonds for dynamic shear moduli of PIB (*30*)]. The dashed blue curve in (G) indicate the best fit to Eq. 1 with $c_\alpha = 10^{-7.9}$ and $c_{SAP} = 10^{-5.2}$. PEMA, poly(ethyl methacrylate).

α-relaxation, $\sim h^{-1}$. As the peak intensity is a direct measurement of the number of units involved in the relaxation process (*2*), we find that both processes originate from the same volume fraction of molecules. These experiments permitted us to verify that a molecular process matching the features required for the Arrhenius processes observed in the equilibration of polymer melts is universally observed in the relaxation dynamics of thin polymer films.

Exploring the relation between the SAP and equilibration processes

We now proceed to a quantitative analysis by comparing the activation energy of the SAP (E_{SAP}) to that of the macroscopic response of nonequilibrated polymer melts (E_A). We start with polyisobutadiene (PIB), whose macroscopic nonequilibrium dynamics was investigated via rheological measurements (*30*). Application of shear induces partial disentanglement of the polymer chains that persists for a short time after removing the shear. This nonequilibrium kinetics follows the process of reentanglement, although it takes places on much shorter time scales. In Fig. 2H, we plotted the reentanglement rate for bulk melts of PIB together with the relaxation time of the SAP observed in the microscopic dynamics of the same polymer, measured at different temperatures. Same as for the other polymers, molecular and equilibration times were plotted on a logarithmic scale, as a function of the inverse temperature; such representation provides a direct access to the activation energy of the processes. Both datasets can be described by linear trends of identical slope, which confirms that the macroscopic nonequilibrium kinetics has the same activation energy (E_{SAP} = 80 ± 10 kJ mol^{-1}, E_A=82 ± 15 kJ mol^{-1})—and, hence, the same molecular origin—of the SAP. While these correlations are notable, more cases should be considered to ensure the universality of the trend.

We searched for similar reports in bulk melts, but the current literature lacks studies over a broad temperature range permitting to extract the value of E_A. Nevertheless, considering the thin polymer films prepared by spin-coating permitted us to extend our analysis to a larger number of different molecules and to further

verify the intimate correlation between equilibration kinetics and SAPs. Thin spin-coated films are, in fact, an archetypical system to investigate nonequilibrium effects (*31*). The fast-processing conditions used—spin-coated layers are obtained within few tens of seconds upon rapid evaporation of diluted polymer solutions—induce persistent mechanical stresses and retard the formation of entangled polymer networks as dense as in bulk melts (*32*). Recovery of equilibrium conditions in these nanolayers has been largely investigated via nanorheological measurements (viscoelastic dewetting) (*17*) and by monitoring the evolution of interfacial properties (irreversible adsorption) (*2*, *3*, *33*). We exploited these studies to investigate equilibration phenomena over a larger number of polymers.

In Fig. 2, we plot the SAP relaxation times (left axis) and the value of the equilibration times (right axis) independently measured in macroscopic experiments, over a large temperature range (see fig. S4 for the relaxation/equilibration maps of other polymers and table S2 for a full list of the equilibration processes used in our analysis and their activation energies). For the different polymer systems investigated, within the experimental uncertainties, the activation energy of the macroscopic kinetics matches that of the SAP (see Fig. 3), as noted above for bulk melts of PIB. The universal character of these trends is further confirmed by previous work, highlighting a correlation between the activation energy of nanorheological measurements and that of several other equilibration mechanisms in thin films of polystyrene (*18*), the most investigated system. It is clear that different equilibration mechanisms share a common molecular origin. Here, we identify such an underlying molecular process with the SAP.

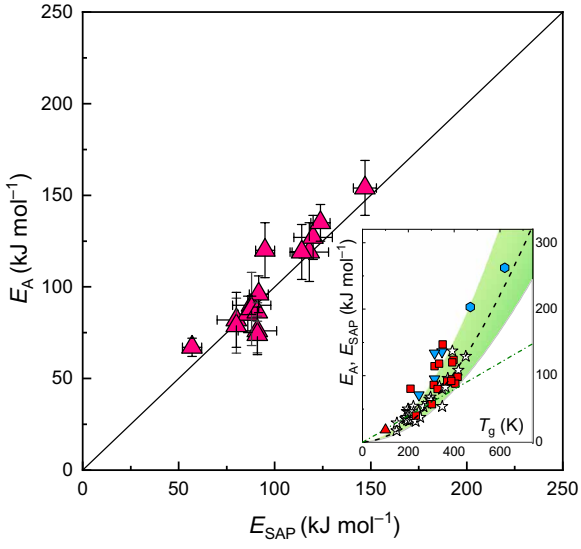

Fig. 3. Correlation between the activation energy of equilibration processes and that of the SAP. The activation energy of several equilibration processes (see Fig. 2 and table S2), is plotted as a function of the activation energy of the SAP (pink triangles); the solid line is the linear function of slope 1 and intercept 0. Inset: Values of activation energy—of both molecular and equilibration processes—as a function of the glass transition temperature; the black dashed line and the green shaded zone represent the expected trend for the mean value and the spread of the high-temperature limit of the activation energy of structural relaxation as a function of T_g, respectively (see the Supplementary Materials). White stars indicate the activation energy of flow for polymer melts at T_g + 150 K (*58*); red squares indicate the activation energy of the SAP in polymers; the red triangle indicates the activation energy of a slow process resembling the SAP, observed by both mechanical and dielectric spectroscopy in ethylcyclohexane (*41*); blue inverted triangles correspond to equilibration processes—surface smoothening and crystallization—of small organic molecules (*15*); and blue hexagons correspond to the mechanical response of metallic glasses (*42*).

DISCUSSION

On the basis of our experimental findings and in line with recent literature (*34*), we draw a scenario in which two relaxation processes coexist in the liquid state: one cooperative mechanism (segmental mobility, associated to the well-known α-relaxation) involving regions of growing length scale upon cooling and another mechanism (SAP) not requiring interaction among relaxing units. Both segmental and Arrhenius processes contribute to the equilibration of the melt, with efficiencies depending on the molecular rearrangements through which free energy is minimized. As in the case of kinetics proceeding via multiple dynamical pathways, according to our scenario, the overall equilibration rate is given by

$$\frac{1}{t_{eq}} = \frac{c_{SAP}}{\tau_{SAP}} + \frac{c_\alpha}{\tau_\alpha} \quad (1)$$

where τ_{SAP} and τ_α indicate the most probable relaxation times of the SAP and the structural (α-)process, respectively. This relation implies that equilibration does not trivially proceed via the fastest molecular process. Efficiency, a quantity inversely proportional to the number of molecular times necessary to equilibrate, should also be considered. Equation 1 can describe different equilibration scenarios both in the liquid and in the glassy state. In particular, for $c_{SAP}/c_\alpha \ll \tau_{SAP}/\tau_\alpha$, we get $t_{eq} \sim \tau_\alpha$, that is, equilibration predominantly follows the conventional structural relaxation; for $c_{SAP}/c_\alpha \gg \tau_{SAP}/\tau_\alpha$, a condition that can occur also at $T > T_g$, equilibration is, instead, driven by the SAP. Regardless of the relative efficiency of the two molecular processes, equilibration at sufficiently low temperatures, where τ_α becomes much greater than τ_{SAP}, e.g., in the glassy state, does strictly follow the activation energy of the SAP in the melt. The SAP should, hence, be responsible for the fast equilibration mechanisms observed in the glassy state.

This idea is in line with the outcome of our results on the equilibration of poly(tertbutyl methacrylate) (PTBMA) (see Fig. 2G). It is remarkable how the presence of the SAP permits the formation of an equilibrated interfacial layer 30 K below T_g within just 1 month, while at the same temperature equilibration through the structural process would require geological times (>10^{11} years). A similar trend is observed for the physical aging of poly(4-tertbutyl styrene) (PTBS) (*14*), PS (*13*), and poly(methyl methacrylate) (PMMA) (*35*), where structural recovery (densification) below T_g proceeds with the same temperature dependence of the SAP (see Fig. 2D). As emphasized above, these results show that measurements of molecular dynamics at temperatures above the glass transition can predict the activation energy of the equilibration processes in the glassy state.

We remark, however, that observing such condition might require performing experiments down to sufficiently low temperatures well below T_g. While the SAP is characterized by one single relaxation time, the structural α-relaxation span over a much larger distribution in relaxation times. Because of the latter condition (not considered in the simple form of Eq. 1), the transition from the super-Arrhenius to the Arrhenius equilibration mechanism can spread over a large temperature window. Analysis of the relaxation/equilibration maps of Fig. 2 shows that PTBMA and PS already

reach the SAP-dominated regime at T_g − 10 K [here, we considered $\tau_\alpha(T_g)$ = 100 s]. For PTBS and PMMA, this condition is reached only at T_g − 25 K, meaning after a further temperature drop by ≈15 K. In the case of PC, for which aging measurements are available down to T_g − 20 K, we could not find clear evidence of the Arrhenius region in the glassy state.

On the basis of the strong connections highlighted in the previous sections and on the notable correlation between the activation energies of the macroscopic equilibration mechanisms, E_A, and of the SAP, E_{SAP} (see Figs. 2 and 3), we anticipate a discussion on the molecular origin of the SAP. We discard any hypothesis related to mechanisms involving secondary processes of the glassy state (−β, −γ, …). Above T_g, secondary relaxations tend to speed up and eventually disappear before reaching temperatures where their characteristic time would exceed that of segmental motion. In addition to that, SAPs are more highly activated than secondary relaxations, e.g., for PMMA (*36*), $E_{SAP} \approx 1.6E_\beta \approx 3.3E_\gamma$ (see also the discussion on the results in the inset of Fig. 3, later in the text).

Our investigation shows that SAPs are characterized by two peculiar features—extremely sharp relaxation peaks and constant activation energy—typical of the dynamic response of a liquid at very high temperatures (>1.3 to 1.4 T_g). In this low-viscosity (≈1 Pa s) regime, differently than in the case of ultraviscous liquids approaching T_g (>1 GPa s), the dynamics is purely exponential—that is, they are described by a single relaxation time as for SAPs—and noncooperative, meaning that they are associated with a temperature-independent activation energy. We thus considered whether SAPs are the manifestation of an ensemble of molecules where relaxation is facilitated with a lack of local constraints, such that molecular rearrangements do not require cooperative motion, such as those at the origin of flow at high temperature. Such relaxation modes should not depend on structure, which would ensure a constant activation energy, regardless of the thermodynamic state (temperature and pressure) of the system.

These hypotheses imply that the SAP and, hence, the mechanisms permitting fast equilibration in the glassy state should resemble segmental mobility in the limit of high temperatures. Our reasoning is verified by the observation that E_{SAP} and E_A match with the expected high-temperature values of the activation energy of the structural process (see the inset of Fig. 3), as quantified by empirical correlations based on T_g (see the Supplementary Materials for derivation). The spread on the data is related to the varying sensitivity to vitrification, quantified in terms of dynamic fragility (shaded green zone; see the Supplementary Materials): At equal T_g, stronger liquids are expected to have a higher activation energy (*37*). We stress that such trend is different than the scaling proposed for secondary relaxations, where either no correlation or a linear relation with T_g is, instead, observed (*38*). For comparison, we added to Fig. 3 the expected scaling of the upper value of the activation energy of secondary processes (green dashed line).

While the experimental results collected so far (identified by features in the dielectric spectra) do not permit providing a mechanistic picture of the molecular rearrangements inducing the SAP, we can extract useful information by analyzing the impact of nanoscopic confinement. The SAP molecular time is invariant upon thickness reduction also in systems where confinement sped up the structural process (see P4ClS and PC in Fig. 2). These findings suggest that the relaxing unit of the SAP is smaller than that of the structural process (1 to 4 nm) and that the former is less (or not at all) sensitive to changes in the structure [density (*39*) and local order (*40*)] imposed by interfaces.

Last, we emphasize that our discussion does not invoke the macromolecular nature of polymers—τ_{SAP} is insensitive to molecular weight—and the intimate relationship between equilibration and SAP should hold independently on the chemical nature of the nonequilibrium system. SAPs have been observed, both via dielectric and mechanical spectroscopy, in a family of 13 small molecules whose structure includes the cyclohexyl group (*41*). The process was associated to an intramolecular transition involving a change in dipole moment. While further investigation is necessary, we verified that the activation energy observed in equilibration mechanisms of nonpolymeric systems—such as the surface diffusion (< T_g) and crystal growth (> T_g) of small organic molecules (*15*, *16*) and the mechanical response (< T_g) of bulk glassy metals (*42*)—follows the same trend that we found for spin-coated polymer films (see inset of Fig. 3).

MATERIALS AND METHODS

Dielectric measurements

Broadband dielectric spectroscopy (BDS) measurements (*43*) were performed using nanocapacitors (*44*), consisting of polymer films (dielectric medium) sandwiched between two aluminum electrodes (see fig. S1). The lower electrode consists of thermally evaporated aluminum layers (Sigma-Aldrich; purity level higher than 99.9%, thickness ≈ 50 nm) deposited onto circular glass substrates. Deposition is performed at stable evaporation rate (≈10 nm s^{-1}), which provided a constant roughness (≈2 nm). The dielectric films (see table S1) were directly spin-coated onto the lower electrode from a solution of the polymer in chloroform or toluene (according to the solubility characteristics of each material). Before deposition, the solution was processed by pressing through 0.4-μm polytetrafluoroethylene filters. Samples were spin-coated at a constant spinning rate (3000 rpm). Tests on P4ClS, a polymer whose dynamics is particularly sensitive to changes in the specific volume (*3*, *45*) and preparation conditions (*46*–*48*), revealed that the spinning rate does not affect molecular dynamics.

To control the spin-coated film thickness, d, we used polymer concentration ranging between 0.5 and 5%. After spin-coating, the polymer films were held for >10^4 times the segmental time at 10 K above bulk T_g (corresponding to the temperature at which, for bulk samples, the segmental time reaches 100 s). Next, the upper surfaces of the films were coated with an additional 50-nm aluminum layer, serving as the upper electrode (fig. S1). Film thickness was calculated from the measured capacitance at room temperature in an approximation of parallel plate geometry, $C_\infty = \varepsilon_\infty\varepsilon_0 (S/d)$, where C_∞ and ε_∞ indicate the capacitance of the film and the dielectric constant of the polymer ε_∞, respectively, in the absence of polarization processes ($T << T_g$) and high frequencies; ε_0 is the vacuum permittivity (8.85×10^{-12} F m^{-1}); and S corresponds to the surface area of the electrodes, which is measured by optical microscopy (typically around 4×10^{-6} m^2).

Complex capacitances were measured in isothermal conditions as a function of the frequency, f, of the electric field in helium environment, using an impedance analyzer (ModuLab XM MTS, Solartron Analytical). Dielectric spectra were obtained from measurements of the capacitance, considering the relaxation $\varepsilon(f) = C(f)d\varepsilon_0^{-1}S^{-1}$.

To extract quantitative information, the isothermal dielectric spectra were analyzed as the sum of the different contributions, including an empirical Havriliak-Negami (HN) (*49*) function for the segmental process and a Cole-Cole (*43*) function for the SAP

$$\varepsilon(\omega) = \varepsilon_\infty + \frac{\Delta\varepsilon_\alpha}{[1 + (i\omega\tau_{HN})^{a_{HN}}]^{b_{HN}}} + \frac{\Delta\varepsilon_{SAP}}{1 + (i\omega\tau_{SAP})^{a_{SAP}}} + \frac{i\sigma}{\varepsilon_0\omega^n} \quad (2)$$

$$\tau_\alpha = \tau_{HN}\left[\sin\frac{a_{HN}\pi}{2 + 2b_{HN}}\right]^{-\frac{1}{a_{HN}}}\left[\sin\frac{a_{HN}b_{HN}\pi}{2 + 2b_{HN}}\right]^{\frac{1}{a_{HN}}} \quad (3)$$

where $\omega = 2\pi f$; ε_∞ is the dielectric constant; τ_{HN} is HN time; $\Delta\varepsilon_\alpha$ is the dielectric strength is of the segmental (α-)process; a_{HN} and b_{HN} are the shape parameters related to the width and the asymmetry of the alpha-peak, respectively; $\Delta\varepsilon_{SAP}$ is the dielectric strength of the SAP; $a_{SAP} \cong 1$ (see further discussion in the Supplementary Materials and fig. S3); σ is the conductivity; and $n \leq 1$. On the high-frequency side of the experimental window, an extra peak shows that negligible temperature dependence is commonly detected in thin-film nanocapacitor geometry. Such peak, easily modeled with a Debye contribution, is an electronic artifact arising from the parasitic resistor-capacitor (RC) circuit due to nonnegligible resistance of metallic contacts (*50*). Differently than the SAP, the parasitic peak is temperature independent (zero activation energy) but moves upon confinement toward the low-frequency side, as the frequency of the maximum of this peak, ~RC, decreases upon thickness reduction ($C \sim d^{-1}$). Examples of deconvolution of the dielectric spectra according to the sum of the abovementioned contributions are shown in fig. S1.

Determination of the adsorption rate via ellipsometry

The polymer solution, prepared in a similar way as for BDS measurements, were spin-coated on top of clean silicon wafers (Si <100> covered by a native oxide layer, ≈2 nm), previously rinsed with acetone, followed by isopropanol, and finally toluene to remove surface contaminants. Our samples are spin-coated at a constant spinning rate (3000 rpm). The thickness of the layer is controlled through polymer concentration and set to a range between 200 and 500 nm to ensure bulk conditions (>7 R_g) (*51*). Spin-coated wafers were then cut into pieces of approximately 1 cm^2 and annealed on a hot plate at controlled temperatures for different annealing times to trigger the adsorption of polymer chains onto the substrate surface. After annealing, the excess polymer (unadsorbed chains) is washed off with the same solvent used to prepare the spin-coated solutions, following Guiselin's experiment (*52*). The procedure exposes the adsorbed layers to the environment.

The thickness of the adsorbed layers was determined immediately after the abovementioned procedure, via ellipsometry. We recorded the ellipsometry angles Ψ and Δ at wavelengths λ between 430 and 850 nm and fitted them to a model considering bulk optical properties, consisting of air/polymer/oxide/substrate. The thickness of silicon oxide layer is measured in the used wafers before deposition of the organic layer. This value is introduced in the optical model as a fixed parameter, which permits to increase the accuracy in the determination of the polymer-adsorbed layer thickness. During the fitting, the density of the adsorbed layer is considered to be the same as in bulk, an approximation (<5%) validated by previous work (*53*, *54*). Typical values of adsorbed layer thickness, h_{ads}, range between 2 and 15 nm (<R_g).

To determine the adsorption rate, we considered that, at short times, the kinetics of irreversible adsorption at the interface between polymer layer and substrate proceeds via two consecutive regimes (*20*, *51*). The first regime, taking place at short times, corresponds to a zero-order reaction mechanism, whose velocity ($\partial h_{ads}/\partial t$) is proportional to the adsorption rate. Further information on the adsorption kinetics is given in the Supplementary Materials.

SUPPLEMENTARY MATERIALS

Supplementary material for this article is available at https://science.org/doi/10.1126/sciadv.abm7154

REFERENCES AND NOTES

1. L. Onsager, Reciprocal relations in irreversible processes. I. *Phys. Rev.* **37**, 405–426 (1931).
2. S. Napolitano, M. Wübbenhorst, The lifetime of the deviations from bulk behaviour in polymers confined at the nanoscale. *Nat. Commun.* **2**, 260 (2011).
3. A. Panagopoulou, S. Napolitano, Irreversible adsorption governs the equilibration of thin polymer films. *Phys. Rev. Lett.* **119**, 097801 (2017).
4. P. G. Debenedetti, F. H. Stillinger, Supercooled liquids and the glass transition. *Nature* **410**, 259–267 (2001).
5. J. Magill, D. Plazek, Crystallization kinetics of 1: 3: 5 tri-α-naphthyl benzene. *Nature* **209**, 70–71 (1966).
6. P. G. de Gennes, Reptation of a polymer chain in the presence of fixed obstacles. *J. Chem. Phys.* **55**, 572–579 (1971).
7. E. W. Fischer, Light scattering and dielectric studies on glass forming liquids. *Phys. A* **201**, 183–206 (1993).
8. X. Monnier, S. Napolitano, D. Cangialosi, Direct observation of desorption of a melt of long polymer chains. *Nat. Commun.* **11**, 4354 (2020).
9. L. Berthier, G. Biroli, J. P. Bouchaud, L. Cipelletti, D. E. Masri, D. L'Hôte, F. Ladieu, M. Pierno, Direct experimental evidence of a growing length scale accompanying the glass transition. *Science* **310**, 1797–1800 (2005).
10. G. Adam, J. H. Gibbs, On the temperature dependence of cooperative relaxation properties in glass-forming liquids. *J. Chem. Phys.* **43**, 139–146 (1965).
11. G. Reiter, M. Hamieh, P. Damman, S. Sclavons, S. Gabriele, T. Vilmin, E. Raphaël, Residual stresses in thin polymer films cause rupture and dominate early stages of dewetting. *Nat. Mater.* **4**, 754–758 (2005).
12. S. Chandran, G. Reiter, Segmental rearrangements relax stresses in nonequilibrated polymer films. *ACS Macro Lett.* **8**, 646–650 (2019).
13. D. Cangialosi, V. M. Boucher, A. Alegria, J. Colmenero, Direct evidence of two equilibration mechanisms in glassy polymers. *Phys. Rev. Lett.* **111**, 095701 (2013).
14. X. Monnier, D. Cangialosi, Thermodynamic ultrastability of a polymer glass confined at the micrometer length scale. *Phys. Rev. Lett.* **121**, 137801 (2018).
15. C. Huang, S. Ruan, T. Cai, L. Yu, Fast surface diffusion and crystallization of amorphous griseofulvin. *J. Phys. Chem. B* **121**, 9463–9468 (2017).
16. J. Alie, C. Lacabanne, J. Menegotto, P. Cardon, H. Duplaa, A. Caron, M. Bauer, Dielectric study of the molecular mobility and the isothermal crystallization kinetics of an amorphous pharmaceutical drug substance. *J. Pharm. Sci.* **93**, 218–233 (2004).
17. M. Chowdhury, P. Freyberg, F. Ziebert, A. C. M. Yang, U. Steiner, G. Reiter, Segmental relaxations have macroscopic consequences in glassy polymer films. *Phys. Rev. Lett.* **109**, 136102 (2012).
18. S. Chandran, R. Handa, M. Kchaou, S. A. Akhrass, A. N. Semenov, G. Reiter, Time allowed for equilibration quantifies the preparation induced nonequilibrium behavior of polymer films. *ACS Macro Lett.* **6**, 1296–1300 (2017).
19. M. Solar, K. Binder, W. Paul, Relaxation processes and glass transition of confined polymer melts: A molecular dynamics simulation of 1,4-polybutadiene between graphite walls. *J. Chem. Phys.* **146**, 203308 (2017).
20. D. N. Simavilla, W. Huang, P. Vandestrick, J. P. Ryckaert, M. Sferrazza, S. Napolitano, Mechanisms of polymer adsorption onto solid substrates. *ACS Macro Lett.* **6**, 975–979 (2017).
21. D. Montarnal, M. Capelot, F. Tournilhac, L. Leibler, Silica-like malleable materials from permanent organic networks. *Science* **334**, 965–968 (2011).
22. M. Tress, E. U. Mapesa, W. Kossack, W. K. Kipnusu, M. Reiche, F. Kremer, Glassy dynamics in condensed isolated polymer chains. *Science* **341**, 1371–1374 (2013).
23. A. Alegría, O. Mitxelena, J. Colmenero, On the molecular motions originating from the dielectric γ-relaxation of bisphenol-A polycarbonate. *Macromolecules* **39**, 2691–2699 (2006).
24. P. Debye, Zur Theorie der anomalen Dispersion im Gebiete der langwelligen elektrischen Strahlung. *Verh dtsch phys Ges* **15**, 777–793 (1913).
25. C. Bottcher, *Theory of Dielectric Polarization* (Elsevier Amsterdam, 1973).

26. V. Lupascu, S. J. Picken, M. Wübbenhorst, Dynamics of T2G2 helices in atactic and syndiotactic polystyrene: New evidence from dielectric spectroscopy and FTIR. *Macromolecules* **39**, 5152–5158 (2006).
27. P. Papon, J. Leblond, P. H. Meijer, *Physics of Phase Transitions* (Springer, 2002).
28. J. M. Schultz, Effect of specimen thickness on crystallization rate. *Macromolecules* **29**, 3022–3024 (1996).
29. P. Rouse Jr., A theory of the linear viscoelastic properties of dilute solutions of coiling polymers. *J. Chem. Phys.* **21**, 1272–1280 (1953).
30. D. Roy, C. Roland, Reentanglement kinetics in polyisobutylene. *Macromolecules* **46**, 9403–9408 (2013).
31. G. Reiter, P. G. de Gennes, Spin-cast, thin, glassy polymer films: Highly metastable forms of matter. *Eur. Phys. J. E* **6**, 25–28 (2001).
32. G. Reiter, The memorizing capacity of polymers. *J. Chem. Phys.* **152**, 150901 (2020).
33. S. Napolitano, *Non-equilibrium Phenomena in Confined Soft Matter* (Springer, 2015).
34. D. M. Sussman, S. S. Schoenholz, E. D. Cubuk, A. J. Liu, Disconnecting structure and dynamics in glassy thin films. *Proc. Natl. Acad. Sci.* **114**, 10601–10605 (2017).
35. V. M. Boucher, D. Cangialosi, A. Alegría, J. Colmenero, Enthalpy recovery of glassy polymers: Dramatic deviations from the extrapolated liquidlike behavior. *Macromolecules* **44**, 8333–8342 (2011).
36. N. G. McCrum, B. E. Read, G. Williams, *Anelastic and Dielectric Effects in Polymeric Solids* (John Wiley, 1967).
37. V. Novikov, A. Sokolov, Poisson's ratio and the fragility of glass-forming liquids. *Nature* **431**, 961–963 (2004).
38. K. Ngai, S. Capaccioli, Relation between the activation energy of the Johari-Goldstein β relaxation and T g of glass formers. *Phys. Rev. E* **69**, 031501 (2004).
39. R. P. White, J. E. Lipson, To understand film dynamics look to the bulk. *Phys. Rev. Lett.* **125**, 058002 (2020).
40. K. Watanabe, T. Kawasaki, H. Tanaka, Structural origin of enhanced slow dynamics near a wall in glass-forming systems. *Nat. Mater.* **10**, 512–520 (2011).
41. A. Mandanici, W. Huang, M. Cutroni, R. Richert, Dynamics of glass-forming liquids. XII. Dielectric study of primary and secondary relaxations in ethylcyclohexane. *J. Chem. Phys.* **128**, 124505 (2008).
42. P. Luo, P. Wen, H. Bai, B. Ruta, W. Wang, Relaxation decoupling in metallic glasses at low temperatures. *Phys. Rev. Lett.* **118**, 225901 (2017).
43. F. Kremer, A. Schoenhals, *Broadband Dielectric Spectroscopy* (Springer, 2003).
44. S. Napolitano, S. Capponi, B. Vanroy, Glassy dynamics of soft matter under 1D confinement: How irreversible adsorption affects molecular packing, mobility gradients and orientational polarization in thin films. *Eur. Phys. J. E* **36**, 37 (2013).
45. K. Adrjanowicz, R. Winkler, A. Dziena, M. Paluch, S. Napolitano, Connecting 1D and 2D confined polymer dynamics to its bulk behavior via density scaling. *ACS Macro Lett.* **8**, 304–309 (2019).
46. S. Napolitano, M. Wübbenhorst, Slowing down of the crystallization kinetics in ultrathin polymer films: A size or an interface effect? *Macromolecules* **39**, 5967–5970 (2006).
47. A. Debot, P. Tripathi, S. Napolitano, Solution filtering affects the glassy dynamics of spincoated thin films of poly(4-chlorostyrene). *Eur. Phys. J. E* **42**, 102 (2019).
48. A. Panagopoulou, C. Rodríguez-Tinoco, R. P. White, J. E. G. Lipson, S. Napolitano, Substrate roughness speeds up segmental dynamics of thin polymer films. *Phys. Rev. Lett.* **124**, 027802 (2020).
49. S. Havriliak, S. Negami, A complex plane representation of dielectric and mechanical relaxation processes in some polymers. *Polymer* **8**, 161–210 (1967).
50. G. Blum, F. Kremer, T. Jaworek, G. Wegner, Molecular dynamics of poly(gamma-octadecyl-co-methyl-L-glutamate) in ultrathin films and in the bulk. *Adv. Mater.* **7**, 1017–1020 (1995).
51. D. N. Simavilla, W. Huang, C. Housmans, M. Sferrazza, S. Napolitano, Taming the strength of interfacial interactions via nanoconfinement. *ACS Cent. Sci.* **4**, 755–759 (2018).
52. S. Napolitano, Irreversible adsorption of polymer melts and nanoconfinement effects. *Soft Matter* **16**, 5348–5365 (2020).
53. C. Housmans, M. Sferrazza, S. Napolitano, Kinetics of irreversible chain adsorption. *Macromolecules* **47**, 3390–3393 (2014).
54. M.-L. Braatz, L. I. Melendez, M. Sferrazza, S. Napolitano, Unexpected impact of irreversible adsorption on thermal expansion: Adsorbed layers are not that dead. *J. Chem. Phys.* **146**, 203304 (2017).
55. R. Richert, Scaling vs. Vogel–Fulcher-type structural relaxation in deeply supercooled materials. *Phys. A* **287**, 26–36 (2000).
56. D. Cangialosi, V. M. Boucher, A. Alegria, J. Colmenero, Free volume holes diffusion to describe physical aging in poly(mehtyl methacrylate)/silica nanocomposites. *J. Chem. Phys.* **135**, 014901 (2011).
57. N. G. Perez-De-Eulate, D. Cangialosi, Double mechanism for structural recovery of polystyrene nanospheres. *Macromolecules* **51**, 3299–3307 (2018).
58. J.-s. Wang, R. S. Porter, On the viscosity-temperature behavior of polymer melts. *Rheol. Acta* **34**, 496–503 (1995).

Acknowledgments: S.N. is thankful for inspiring discussions on dynamics and equilibration mechanisms with D. Cangialosi, S. Chandran, L. Grassia, V. Lupaşcu, G. Reiter, R. White, and M. Wübbenhorst. **Funding:** The authors acknowledge financial support from the Fonds de la Recherche Scientifique FNRS under grant T.0184.20 "EXOTICAGE," from Action de Recherche Concertée—ULB under grant ARC 20061 "SADI," and from the Fondation Jaumotte-Demoulin under grant "DUDELA-2021." Z.S. is thankful to the China Scholarship Council for doctoral grant CSC 201807565008. **Author contributions:** S.N. conceived the idea, designed the experiments, and secured the funding. Z.S. and C.R.-T. prepared the samples and performed most of the experiments. Z.S. analyzed the adsorption kinetics. C.R.-T. analyzed the dielectric spectra. A.M. performed some experiments and optimized the dielectric setup. S.N., C.R.-T., and Z.S. wrote the manuscript. All authors contributed to the discussion of the results. **Competing interests:** The authors declare that they have no competing interests. **Data and materials availability:** All data needed to evaluate the conclusions in the paper are present in the paper and/or the Supplementary Materials.

Submitted 7 October 2021
Accepted 1 March 2022
Published 15 April 2022
10.1126/sciadv.abm7154

ScienceAdvances

Fast equilibration mechanisms in disordered materials mediated by slow liquid dynamics

Zijian SongCristian Rodríguez-TinocoAllen MathewSimone Napolitano

Sci. Adv., 8 (15), eabm7154. • DOI: 10.1126/sciadv.abm7154

Science Advances (ISSN) is published by the American Association for the Advancement of Science. 1200 New York Avenue NW, Washington, DC 20005. The title *Science Advances* is a registered trademark of AAAS.